Miniature Optical Fiber Photoacoustic Gas Sensor Based on a 3D Micro-Printed Ferrule-Top Optomechanical Resonator

Taige Li[1,†], Pengcheng Zhao[1,†], Peng Wang[1], Kummara Venkata Krishnaiah[1], Wei Jin[1,*], and A. Ping Zhang[1,2,*]

[1] Photonics Research Institute, Department of Electrical and Electronic Engineering, The Hong Kong Polytechnic University, Kowloon, Hong Kong SAR, China.

[2] State Key Laboratory of Ultraprecision Machining Technology, The Hong Kong Polytechnic University, Kowloon, Hong Kong SAR, China

[†] These authors contributed equally to this work.

*Email: azhang@polyu.edu.hk (A.P.Z.); eewjin@polyu.edu.hk (W.J.)

ABSTRACT

We present a small-size high-sensitivity optical fiber photoacoustic gas sensor based on a sub-millimeter optomechanical resonator (OMR) that is directly 3D micro-printed on the end-face of a fiber-optic ferrule. The 3D micro-printed OMR and the end-face of the optical fiber form a low-finesse Fabry-Pérot (FP) microcavity for interferometric acoustic detection, achieving an acoustic sensitivity of 296 mV/Pa. Together with a pump laser beam, an optical fiber OMR-based photoacoustic gas sensor is demonstrated to detect acetylene gas at the concentration level of 137 parts per billion. This highly sensitive and compact optical fiber gas sensor offers a promising solution for trace-gas detection in diverse applications ranging from biomedical diagnostics to in-reactor monitoring.

Keywords: Optical fiber sensor, Photoacoustic gas sensor, Optomechanical microresonator, Fabry-Pérot cavity, 3D micro-printing

1. INTRODUCTION

Trace gas sensors play a very important role in various applications, such as medical diagnosis and environmental surveillance [1-3]. One of the promising gas detection techniques is photoacoustic spectroscopy (PAS) technology, which offers the advantages of compact size, high sensitivity, and fast response [4]. It employs a modulated laser beam whose absorption by a target gas species can generate a weak acoustic wave via photoacoustic (PA) effect, which can be detected by an acoustic sensor for gas analysis. The performance of a PAS gas sensor primarily depends on the acoustic detector's ability in the detection of weak acoustic waves. Conventional PAS systems use millimeter or centimeter-scale microphones, such as capacitive transducers, tuning forks, or silicon cantilevers, and PA cell may be further employed to achieve higher sensitivity in gas detection [5-7]. Therefore, one of the remaining challenges for PAS gas sensing system is the development of miniaturized PAS gas sensors, which could enable their widespread applications in space-constrained circumstances.

Recently, we demonstrated a 3D microprinted fiber-tip spirally-suspended optomechanical resonator (OMR) acoustic detector [8], which addresses the trade-off between compact size and high sensitivity in the detection of acoustic wave. Here, we extend our work to develop a high-sensitivity optical fiber PAS gas sensor using a 3D micro-printed ferrule-top

Advanced Fiber Laser Conference (AFL 2024), edited by Guoqing Chang, Yan Feng, Proc. of SPIE Vol. 13544, 1354410 · © 2025 SPIE
0277-786X · doi: 10.1117/12.3058740

OMR. Compared to the end-face of optical fiber, the fiber-optic ferrule end-face offers a much larger space that allows the fabrication of the OMRs with longer suspending microbeams, resulting in a lower resonant frequency and an enhanced acoustic sensitivity. With an OMR of only 400 μm in diameter, the fabricated optical fiber PAS sensor can detect acetylene (C_2H_2) gas at a concentration of 137 ppb at a resonant frequency of ~19 kHz without the use of a PA cell.

2. DESIGN AND PRINCIPLE

Figure 1(a) shows the schematic design of the optical fiber PAS gas sensor with a spirally-suspended OMR on the end-face of a fiber-optic ferrule. The sensor consists of a polymer microdisk that is supported by three spiral microbeams. The microdisk and optical fiber end-face form a low-fineness Fabry-Pérot interferometer (FPI). The optical fiber FPI sensor can form a PAS gas detection microsystem together with a modulated pump laser, whose wavelength is tuned to an absorption line of the target gas. The absorption of the modulated pump light by gas molecules generates acoustic waves, which can excite the ferrule-top OMR to resonantly vibrate. When the modulation frequency matches with the resonance frequency of the OMR, the vibration amplitude can be resonantly enhanced. The PA-induced cavity length change of FPI can be interferometrically demodulated via a probe light incident into the same FP microcavity. Under weak absorption approximation, the PA signal is given by [9]

$$S = P_{\text{pump}} \cdot \alpha \cdot C \cdot k_{\text{cell}}, \tag{1}$$

where P_{pump} (W) is the pump power, α (cm^{-1}) is the absorption coefficient, C is the concentration of target gas, and k_{cell} ($\text{V}\cdot\text{cm}\cdot\text{W}^{-1}$) is the cell constant that depends on the geometry of the PA cell, the beam profile, the acoustic detector and the nature of acoustic mode.

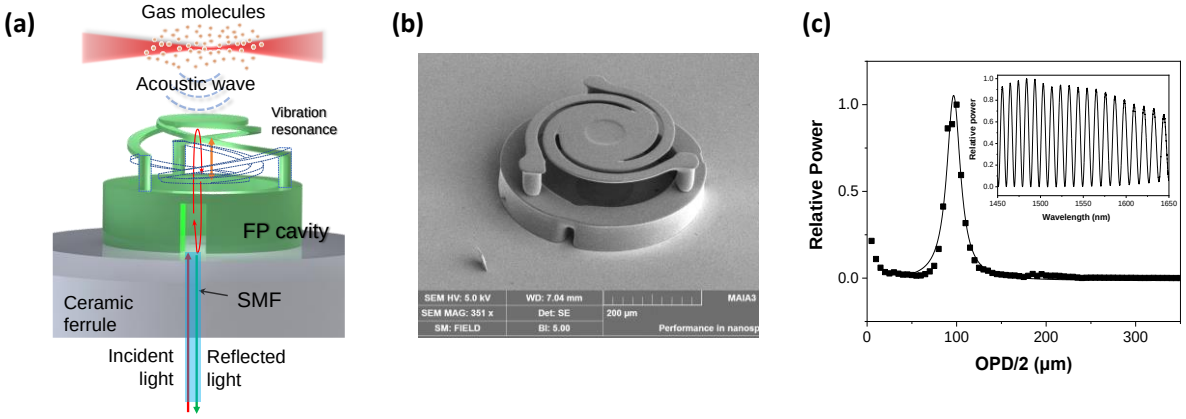

Figure 1. (a) Schematic of a ferrule-top spirally-suspended OMR for PAS gas sensing. (b) SEM image of the fabricated OMR. (c) FFT result of the measured reflection spectrum of the OMR. Inset: the normalized reflection spectrum.

3. EXPERIMENTAL RESULTS

3.1. Fabrication of optical fiber OMR acoustic sensor

The ferrule-top spirally-suspended OMR was fabricated by using our in-house optical 3D micro-printing technology

[10,11]. **Figure** 1(b) shows the SEM image of the fabricated OMR in which a supporting ring base was introduced to increase the length of the FP microcavity. The whole structure has a height of ~100 μm, and its outer diameter is ~400 μm. The thickness and length of the microbeams of the OMR are ~10 μm and ~434 μm, respectively. **Fig**. 1(c) is the fast Fourier transform (FFT) results of the measured reflection spectrum, given in the inset of **Fig**. 1(c), of the fabricated OMR. The free spectral range and fringe contrast of the reflection spectrum of the FP microcavity is ~12.0 nm and ~15 dB, respectively. The cavity length of the FP microcavity obtained from the FFT result is ~100 μm, which agrees well with the design.

3.2. Testing results of the optical fiber OMR sensor's acoustic response

The response of the fabricated optical fiber OMR to acoustic waves in air was tested using a setup similar to that described in Ref. [12]. A piezo loudspeaker (Kemo L010) driven by a signal generator was used to produce acoustic waves. The laser wavelength was tuned to a quadrature point of the OMR's reflection spectrum shown in the inset of **Fig**. 1(c). The reflected light was delivered through an optical circulator, and the light intensity variations were analysed by a digital oscilloscope. To calibrate acoustic signals, a commercial microphone (B&K 4939) was positioned near the OMR acoustic detectors to measure acoustic pressure. All components including the loudspeaker, the OMR sensor, and the microphone were placed in an acoustic isolation box to minimize external noise interference.

Figure 2(a) presents the measured frequency response of the optical fiber OMR to acoustic waves, from which one can see that the first-order resonant vibration mode occurred at ~19.3 kHz. The inset of **Fig**. 2(a) illustrates the measured waveform under 5-Pa acoustic excitation at the resonance frequency. **Fig.** 2(b) shows the measured output intensity as a function of applied acoustic pressure when the sensor operates at resonance and non-resonance conditions. A linear relationship was observed between the output signal and acoustic pressure in both cases. The measured acoustic sensitivity of the optical fiber OMR at the resonance frequency is ~296 mV/Pa, while the sensitivity changed to ~3.3 mV/Pa under off-resonance condition, indicating that resonance can enhance sensitivity by around 90 times.

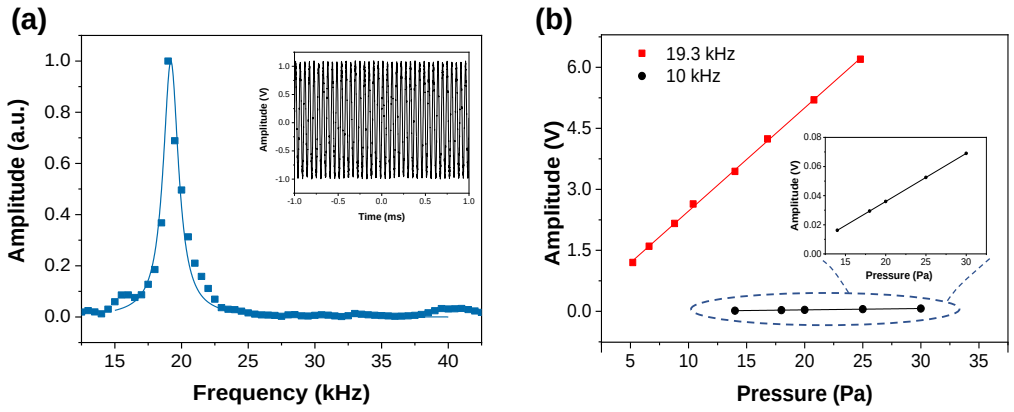

Figure 2. (a) The measured frequency response of the fabricated optical fiber OMR acoustic sensor. The inset is the measured waveform at the resonance frequency of 19.3 kHz. (b) The measured outputs of the optical fiber OMR acoustic sensor with respect to applied acoustic pressure at resonant or non-resonant frequencies.

3.3. Testing results of the optical fiber OMR-PAS gas sensor

The fabricated optical fiber OMR-PAS gas sensor was tested by using a standard pump-probe setup, as depicted in **Fig**. 3.

The pump laser, sourced from a 1533-nm distributed feedback (DFB) laser, was amplified by an erbium-doped fiber amplifier (EDFA). Second harmonic (2*f*) based wavelength modulation technique was applied for gas detection. During the test, the pump laser beam was transmitted via a standard single-mode fiber which was placed perpendicular to the OMR sensor head closely , as shown in the inset of **Fig**. 3. The wavelength of pump laser was gradually scanned across the *P*(13) absorption line of C_2H_2 gas and simultaneously modulated sinusoidally at a frequency *f* of 9.65 kHz to generate acoustic waves.

A probe laser beam from a tunable semiconductor laser (TSL) was employed for the interferometric interrogation of the optical fiber FPI sensor. The probe light coming out from an optical circulator (OC) is detected by a balanced photodetector (BPD) to reduce probe laser intensity noise. The 2*f* component of the probe was demodulated by a lock-in amplifier (LIA, Zurich Instrument MFLI 500 kHz) and transmitted to a computer via a data acquisition (DAQ) card. An error signal, derived from the difference between the DC component of the probe detected by the photodetector (PD) and a reference voltage, was applied to stabilize the probe wavelength at the quadrature point to maximize PAS signal.

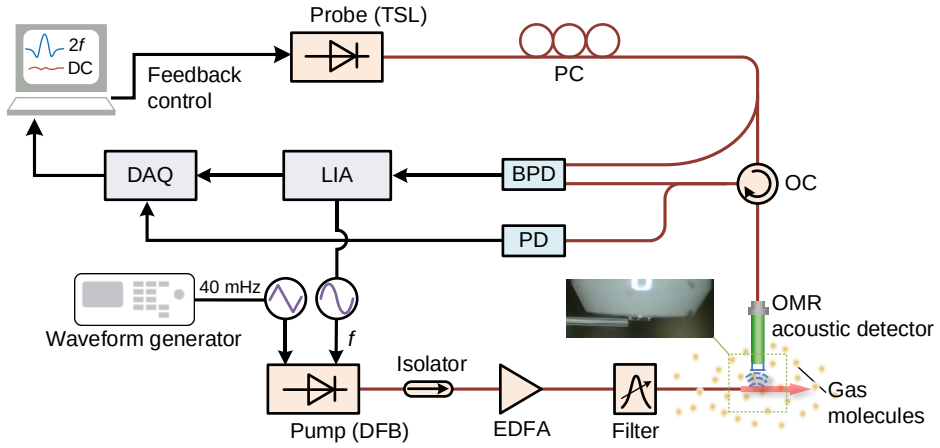

Figure 3. Schematic diagram of the experimental setup for testing the optical fiber OMR-PAS gas sensor. DFB, distributed feedback laser; TSL, tunable semiconductor laser; EDFA, erbium-doped fiber amplifier; PC, polarization controller; OC, optical circulator; BPD, balanced photodetector (PD); LIA, lock-in amplifier; DAQ, data acquisition card.

The detection limit of the optical fiber OMR-PAS gas sensor was tested by continuously injecting N_2-balanced 1000-ppm C_2H_2 to the sensor head. **Figure** 4(a) shows the 2*f* lock-in output signals obtained by scanning the pump wavelength across the *P*(13) line of C_2H_2 at various input pump power levels. The corresponding peak-to-peak values of the 2*f* signal (PAS signal) as a function of input pump power are presented in **Fig**. 4(b), showing a nearly linear increase in PAS signal amplitude with pump power. The system noise was measured with the pump wavelength fixed at the *P*(13) line, while the sensor was exposed to air. **Figure** 4(c) compares the standard deviation of the noise (1σ noise) with and without the pump laser. The 1σ noise values remain nearly identical, indicating minimal noise variation with increasing pump power. At the input pump power of 210 mW, the signal-to-noise ratio for 1-s lock-in time constant was calculated to be ~610 that gives a noise-equivalent concentration (NEC) of 1.64-ppm C_2H_2.

To further assess the minimum NEC of the gas sensor, an Allan-Werle deviation analysis [13,14] was performed using the noise data collected over a period of three hours, as shown in **Fig.** 4(d). When the integration time is less than ~941 s,

the NEC decreases with an increase of integration time. The NEC values are ~484-ppb and ~137-ppb C_2H_2 gas for the integration times of 100 s and 941 s, respectively. According to the above analysis about the relationship between the signal, noise and pump power, the detection sensitivity of the optical fiber OMR-PAS gas sensor is believed to be further improved in case a higher pump power is applied.

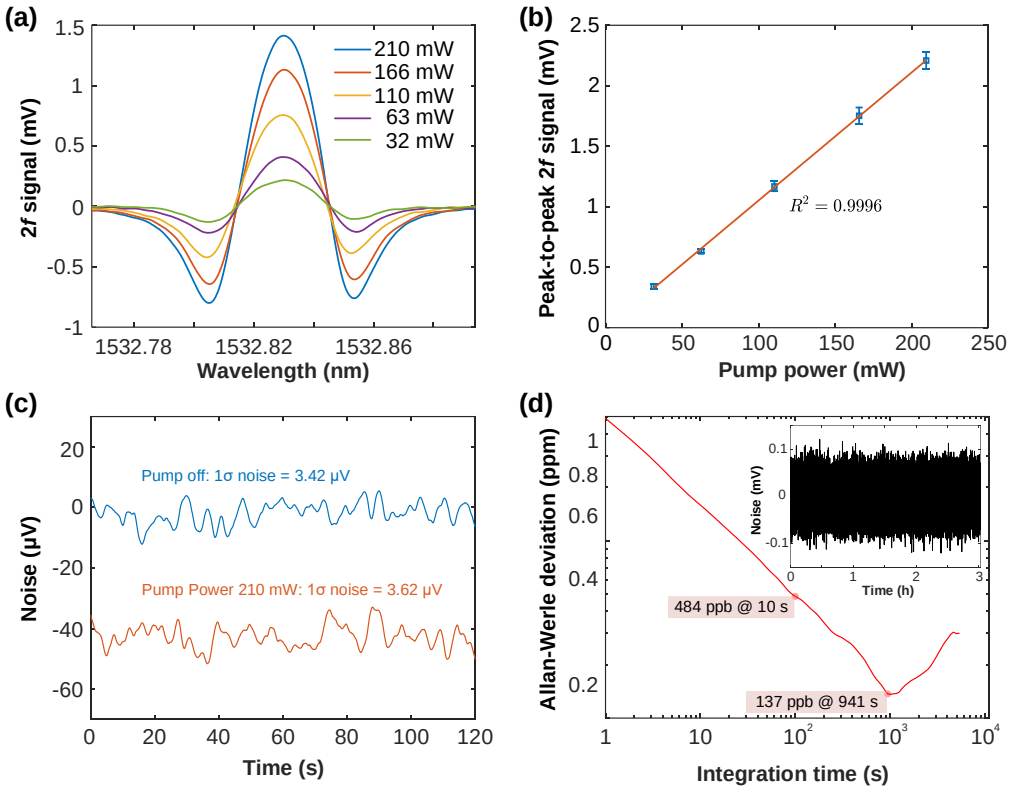

Figure 4. (a) Measured 2*f* signals for 1000-ppm C_2H_2 at different input pump power levels. (b) Peak-to-peak value of the 2*f* signals as a function of input pump power levels. (c) The noise with and without pump laser as a function over a period of 120 s. (d) Allan-Werle deviation plot. The inset is the measured noise over 3 hours.

4. CONCLUSION

In conclusion, we have demonstrated an ultracompact optical fiber PAS gas sensor based on a sub-millimeter OMR that is directly 3D micro-printed on the end-face of a fiber-optic ferrule. The optical fiber OMR-PAS gas sensor has a very small sensor head whose diameter is 400 μm, and it can sensitively detect C_2H_2 gas at the concentration level of 137 ppb without the use of PA cell. This small-size high-sensitivity optical fiber PAS gas sensor provides a new trace-gas detection technology for various applications such as environmental monitoring and industrial process controls.

ACKNOWLEDGEMENTS

The work was supported by the Research Grants Council of the Hong Kong SAR, China (Grant No.: 15221119) and the Local Innovative and Research Teams Project of Guangdong Pearl River Talents Program (Grant No.: 2019BT02X105).

REFERENCES

[1] Mitrayana, Apriyanto D.K., and Satriawan, M., "CO_2 Laser Photoacoustic Spectrometer for Measuring Acetone in the Breath of Lung Cancer Patients," Biosensors **10**(6), 55 (2020).

[2] Stein, L.Y., and Lidstrom, M.E., "Greenhouse gas mitigation requires caution," Science **384**(6700), 1068-1069 (2024).

[3] Zhao, P., Zhao, Y., Bao, H., Ho, H.L., Jin, W., Fan, S., Gao, S., Wang, Y., and Wang, P., "Mode-phase-difference photothermal spectroscopy for gas detection with an anti-resonant hollow-core optical fiber," Nat. Commun. **11**(1), 847 (2020).

[4] Fathy, A., Sabry, Y.M., Hunter, I.W., Khalil, D., and Bourouina, T., "Direct Absorption and Photoacoustic Spectroscopy for Gas Sensing and Analysis: A Critical Review," Laser Photon. Rev. **16**(8), 2100556 (2022).

[5] Huang, Q., Wei, Y., and Li, J., "Simultaneous detection of multiple gases using multi-resonance photoacoustic spectroscopy," Sens. Actuators B Chem. **369**, 132234 (2022).

[6] Qiao, S., He, Y., Sun, H., Patimisco, P., Sampaolo, A., Spagnolo, V., and Ma, Y., "Ultra-highly sensitive dual gases detection based on photoacoustic spectroscopy by exploiting a long-wave, high-power, wide-tunable, single-longitudinal-mode solid-state laser," Light Sci. Appl. **13**(1), 100 (2024).

[7] Guo, M., Chen, K., Li, C., Xu, L., Zhang, G., Wang, N., Li, C., Ma, F., Gong, Z., and Yu, Q., "High-Sensitivity Silicon Cantilever-Enhanced Photoacoustic Spectroscopy Analyzer with Low Gas Consumption," Anal. Chem. **94**(2), 1151-1157 (2022).

[8] Yao, M., Zhang, Y., Ouyang, X., Zhang, A.P., Tam, H.Y., and Wai, P.K.A., "Ultracompact optical fiber acoustic sensors based on a fiber-top spirally-suspended optomechanical microresonator," Opt. Lett. **45**(13), 3516-3519 (2020).

[9] Elia, A., Lugarà, P.M., Franco, C.D., and Spagnolo, V., "Photoacoustic Techniques for Trace Gas Sensing Based on Semiconductor Laser Sources," Sensors **9**(12), 9616-9628 (2009).

[10] Wu, J., Yao, M., Xiong, F., Zhang, A. P., Tam, H.-Y., and Wai, P. K. A., "Optical fiber-tip Fabry-Pérot interferometric pressure sensor based on an in-situ μ-printed air cavity," J. Lightwave Tech. **36**, 3618-3623 (2018).

[11] Zhao, P., Krishnaiah, K.V., Guo, L., Li, T., Ho, H.L., Zhang, A.P., and Jin, W., "Ultraminiature Optical Fiber-Tip 3D-Microprinted Photothermal Interferometric Gas Sensors," Laser Photon. Rev. 2301285 (2024).

[12] Tan, Y., Zhang, C., Jin, W., Yang, F., Ho, H.L., and Ma, J., "Optical fiber photoacoustic gas sensor with graphene nano-mechanical resonator as the acoustic detector," IEEE J. Sel. Top. Quantum Electron. **23**(2), 199-209 (2016).

[13] Allan, D.W., "Statistics of atomic frequency standards," Proc. IEEE **54**(2), 221-230 (1966).

[14] Werle, P.O., Mücke, R., and Slemr, F., "The limits of signal averaging in atmospheric trace-gas monitoring by tunable diode-laser absorption spectroscopy (TDLAS)," Appl. Phys. B **57**, 131-139 (1993).